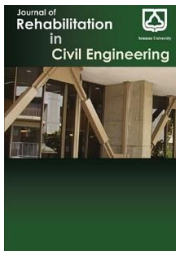

journal homepage: http://civiljournal.semnan.ac.ir/

Calculation of Equivalent Axle Load Factor Based on Artificial Intelligence

Fazel Fasihi[1], Mahmoud Reza Keymanesh[2], Seyyed Ali Sahaf [3], Soheil Ghareh[4]

1. Ph.D. Candidate, Department of Civil Engineering, Payame Noor University, P.O.Box 19395-4697, Tehran, Iran
2. Associate Professor, Department of Civil Engineering, Payame Noor University, P.O.Box 19395-4697, Tehran, Iran
3. Assistant Professor, Faculty of Engineering, Ferdowsi University, P.O.Box 9177948974, Mashhad, Iran
Corresponding author: *mrkeymanesh@pnu.ac.ir*

ARTICLE INFO

Article history:
Received: 12 January 2021
Revised: 14 March 2021
Accepted: 01 May 2021

Keywords:
Pavement;
Equivalent Axle Load Factor;
Finite Element;
ABAQUS;
Artificial Intelligence;

ABSTRACT

In most road pavements design methods, a solution is required to transform the traffic spectrum to standard axle load with using equivalent axle load factor (EALF). The EALF depends on various parameters, but in existing design methods, only the axle type (single, tandem, and tridem) and pavement structure number were considered. Also, the EALF only determined for experimental axles and axle details (i.e., axle weight, length, pressure), wheel type (single or dual wheel) plus pavement properties were overlooked which may cause inaccuracy and unusable for the new axle. This paper presented a developed model based on Artificial Neural Network (ANN) for calculation of EALFs considering axle type, axle length, contact area, pavement structure number (SN), tire pressure, speed, and final serviceability. Backpropagation architecture was selected for the model for the EALF prediction based on fatigue criteria. Finally, among all reviewed ANN configuration, a network with 7-13-1 was selected for the optimum network.

1. Introduction

Preserving pavements in good conditions allow people to drive with acceptable comfort and safety levels. For keeping pavements in good condition, it is essential to gather accurate data by periodical inspection during pavement service life.

One of the most effective parameters for analysis and design of the pavement structures is Traffic information which any

How to cite this article:
Fasihi, F., Keymanesh, M., Sahaf, S., Ghareh, S. (2021). Calculation of Equivalent Axle Load Factor Based on Artificial Intelligence. Journal of Rehabilitation in Civil Engineering, 9(3), 89-100.
https://doi.org/10.22075/JRCE.2021.22366.1475

errors will lead the pavement to fail due to fatigue, rutting, etc.

In most structural design guides for the pavement, traffic loading is defined by ESALs, which is the acronym for equivalent single axle load.

As mentioned in AASHTO manual, ESALs, transforms the different passing loads into the standard axle on the same pavement. The final serviceability index, pavement type, and pavement thickness are the parameters used to calculate the ESAL number. The ESAL used the equivalent axle load factor (EALF) to transform the passing cars with different axles types of into standard axle (18 kips in single axles with dual tires equal to 80 KN) by using Equation (1).

$$ESAL = \sum_{i=1}^{n} EALF_i \times n_i \quad (1)$$

Where i is the number of the axle types, n is the number of axle types, $EALF_i$ is the EALF for ith axle type, and n_i is the number of moves of the ith axle type.

The EALF for flexible pavements based on the results of the AASHTO Experiments (1962) is defined as Equation (2).

$$EALF = \frac{W_{t18}}{W_{tx}} \quad (2)$$

$$\log\left(\frac{Wt_x}{W_{t18}}\right) = 4.79\log(18+1) - 4.79\log(L_x + L_2) + 4.33\log L_2 + \frac{G_t}{\beta_x} - \frac{G_t}{\beta_{18}} \quad (3)$$

$$G_t = \log\left(\frac{4.2 - p_t}{4.2 - 1.5}\right) \quad (4)$$

$$\beta_x = 0.40 + \frac{0.081(L_x - L_2)^{3.23}}{(SN+1)^{5.19} L_2^{3.23}} \quad (5)$$

Where Wt_{18} is the number of passing standard axle (18 kips), Wt_x is the number of passing x-axle, L_x is the load of axle (kips), L_2 is the axle type (single, tandem and tridem axles are respectively 1, 2 and 3), β_{18} is the value of b_x when L_x is equal to 18 and L_2 is equal to 1, p_t is the final serviceability, SN is the structural number.

In the mechanical design method, the EALF is the ratio of the allowable passing for the standard axle and actual load as Equation (6).

$$EALF = \frac{N_{80}}{N_x} \quad (6)$$

Where 80 and x are respectively the 80-kN axle load (standard axle load) and the actual axle load.

Ofcourse, the allowable passing can be calculated as expressed in Equation (7).

$$N = \alpha \times E^{(-b)} \times \varepsilon^{(-C)} \quad (7)$$

where N is the allowable passing before fatigue cracking, E is the modulus of asphalt, ε is the tensile strain at the bottom of the asphalt layer, a, b and c are experimentally constants.

Finally, Equation (8) will be created with incorporation of Equation (7) in Equation (6). It's conducted based on fatigue failure criteria to compute the EALF for all pavement and axle type.

$$EALF = \left(\frac{\varepsilon_x}{\varepsilon_{80}}\right)^c \quad (8)$$

Where ε_x and ε_{80} respectivly are the tensile strain for the actual axle and the standard axle (the 80-kN axle load), and c is experimentally constants.

The main disadvantages of these equations are the disregarding of many effective parameters and restricting to experimental axles in the AASHTO Road Test (1962). Nowadays, development of car production causes to make different axles in every location with different types, pressure and

etc. which not available any comprehensive method to calculate the EALF.

This paper aimed to describe the development of an artificial neural network model of the EALF calculation by focus on the wheel type (single or dual), contact area, tire pressure and pavement properties. Finally, the created model is based on the results of 760 different simulation in ABAQUS finite element software.

2. Literature review

As mentioned above, the main deficiency of AASHTO's EALF equation was the restriction to experimental axles and the inability to cover the variety of new axles, which led us to perform further research on effective parameters of EALF. Some recently important studies stated below.

Zaghloul and White researched the heavy loads impact on the EALF in highways of Indiana based on the permanent deformation of flexible pavements with a three-dimensional finite element method. The results in both of static and dynamic analysis, confirmed that the EALF calculated in that research was according to the AASHTO parameters [1].

Chatti et al. studied on thin, medium, and thick flexible pavements with passing loads of single, tandem, and tridem axles. They calculate EALF based on peak strains, the difference between peak and valley (midway) strains, and dissipated energy with Fatigue Criteria. Results showed under a single axle the critical response is the longitudinal strain. Also, the dissipated energy method compared with the strain-based method gives LEFs that is about 20% and 30% more for tandem and tridem axles, respectively, in thin to medium pavements. For thick pavements, the difference is not significant [2].

AbdelMotaleb studied the EALF variations based on axle load and pressure of high tire with fatigue and rutting criteria for flexible pavement in Egypt. The results showed that the effect of increased tire pressure directly depends on axle load. At low till medium axle loads (less than 17.31 ton), the tire pressure increases causes an increase in EALF, but at high axle loads, the dependency EALF with tire pressure becomes insignificant [3].

Judycki calculated EALF for flexible and semi-rigid pavements based on fatigue criteria. It was found the equivalency factors form fatigue criteria related closely to the fourth power mathematical equation but in semi-rigid pavements are much more complicated [4].

Chaudry and Memon researched on effects of seasonal variation on truck factor in Pakistan. It's founded axle truck type 3 (29.5 Ton single axle and 27.5 Ton tandem axle) is the most endamaging between all truck types with 6.4 times greater than the design truck. The results showed that the calculated polynomial expressions could be used to estimate the truck factor with high accuracy [5].

Amorim et al. tried to model an artificial neural network for predicting EALF and controlled wheel type effects. They found a dual wheel are approximately ten times less than single wheels in the same properties [6].

Four methods of EALF compared by Rys et al. They concluded that the AASHTO 1993, French LCPC and fourth power equation solutions, derivative load equivalency factors at a similar situation and dynamic loads of cars have a significantly hamrful effect on pavement structure [7].

The seasonal effect on EALF in China was studied by Zhang et al. They simulated pavements in 3 seasons and finally modeled

an artificial neural network to predict EALF by seasonal variations [8].

Singh and Sahoo researched on analysis of two asphalt layer in ABAQUS. Their study showed pavement reaction is little dependence on poisson ratio and more on ratio of modulus of pavement and subgrade, pavement thickness and tire width [9].

Flexible pavement deterioration based on moving loads in 3D and 2D axisymmetric at crack propagation step investigated by Deng et al.. In that, time lag between the load and deflection peaks defined as "Lag angle". Their research showed lag angle is depends on degree of deterioration, load speed and material properties [10]. Furthermore, many researchers effectively attempted to employ machine learning-based techniques for characterization of civil engineering systems and construction materials behavior [11–15].

3. Case study

As mentioned, the aim of this research was to develop an ANN network to predict EALF of any axle types. To this end, the three-dimensional finite element (FE) model for the single, tandem, and tridem axle configurations with dynamic loading was used to develop the EALF caused by fatigue criteria.

In Finite element simulation, several important factors such as element type, size, meshing, boundary condition effect on the accuracy of the results. Boundaries in a appropriate geometry model, should not effects on the responses and in dynamic analysis, should minimize the dilatational reaction and energy of shear wave back to the model [16]. For this purpose, 3D with 8 nodes linear brick reduced integration (C3D8R) elements was selected [17–19].

The dimensions of the simulated samples in ABAQUS remarkably impact the values of the results and should be considered so that it minimizes the simulation process duration, in addition to eliminating the reflection wave load effects. On the other hand, the selection of large dimensions makes calculations heavier and the solution process longer, which if the system fails to solve or process, it may deliver no solution or negatively affect the accuracy of the outputs. The optimal dimensions in ABAQUS have been restricted to 20R on each side of the loading surface in the horizontal direction (xy plane) and to 140R in the vertical direction (z-axis), where R is the radius of the loading area [17].

In most conducted researches, a load of vehicles considered to be static, but pavement performance is strongly influenced by dynamic loading [20]. For this reason, load simulation was done dynamically with single and double wheels in single, tandem, and tridem axles. It is worth mentioning, in dual wheels, the distance between the centers of wheels was equal to three times of wheel radius.

Because in this study, the fatigue cracking selected for failure mode; The tensile strain in single axles under the asphalt layer is the result of axle load passing. But for tandem axles, the tensile strain should be considered as two components due to the part of the remained the first axle strain level, and the second axle passing. The same appears for other multiple axles types. To obtained this, the Huang suggested method was used [21]. It's consists of the strains calculation according to the positions showed in Figure 1 and 2, at the single wheel center, at the single wheel edge and at the double wheels center. For the first axle, the strain should be checked under the first axle (ε_a). For the second and other multiple axles, the strain is equal to $\varepsilon_a - \varepsilon_b$; which ε_b is the strain at the midpoint located between two axles [21]. Table (1) and (2) and figure (3) shows the summary of FE simulation details.

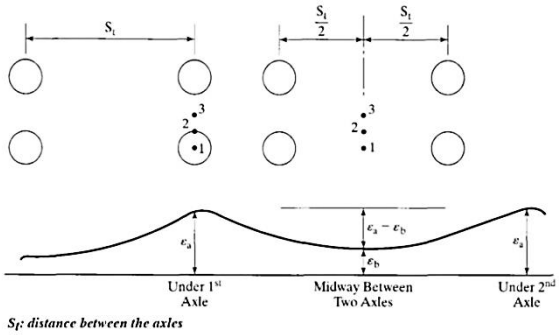

Fig. 1. damage analysis for tandem axles [21].

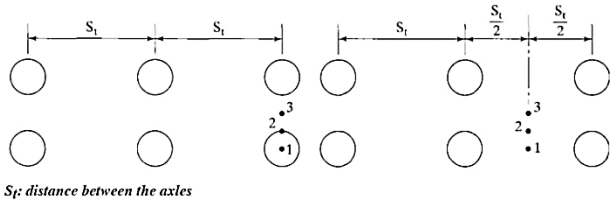

Fig. 2. damage analysis for tridem axles [21].

Table 1. FE simulation details.

Attribute		Description	References used No.
Software		ABAQUS (Ver. 6.14)	
Element type		C3D8R	[17–19]
Simulated section size		20R×20R*	[22]
Simulated height size		140R*	[22]
Boundary condition		Edge of model Roller supports Sub-model fully fixed supports	[20]
Mesh		Variable (finer around load pass)	-
Loading		haversine function 3 – 30 (ton)	[23,24]
Axle types		Single, tandem and tridem	-
Axle Distances (in multiple axles) (m)		1.2 – 1.5	
Tire pressure		400 – 900 KPa	[25]
Load contact radius (m)		0.1 – 0.125	
Loading Frequencies		6 - 14	[26]
Asphalt damping ratio		0 – 15 (%)	[21]
Layer modulus range (MPa)	asphalt	2000 - 12000	
	Base	20 – 120	
	subbase	20 – 120	
	subgrade	20 - 80	
Layer Poisson's ratios	asphalt	0.35	
	Base	0.4	
	subbase	0.4	
	subgrade	0.45	
Layer thickness range (m)	asphalt	0.1 – 0.3	
	Base	0.1 – 0.5	
	subbase	0.1 – 0.6	
Used equation		8	

*) R: loading contact radius

Table 2. Asphalt Shear modulus of models.

mode	Elastic		Viscous				
			n	Gi	Ki	i (s)	τ
1	Elastic modulus (MPa)	9840	1	0.631	0.631	0.078	0.0206
			2	0.251	0.251	0.816	0.173
			3	0.0847	0.0847	5.68	1.29
	Poisson Ratio	0.35	4	0.0266	0.0266	139	5.35
			5	0.00666	0.00666	344	0.0106
2	Elastic modulus (MPa)	18790	1	0.452	0.631	0.003	0.000113
			2	0.278	0.251	0.3	0.00314
			3	0.148	0.0847	3	0.013
	Poisson Ratio	0.35	4	0.108	0.0266	10	0.184
			5	0.00746	0.00666	100	2.29

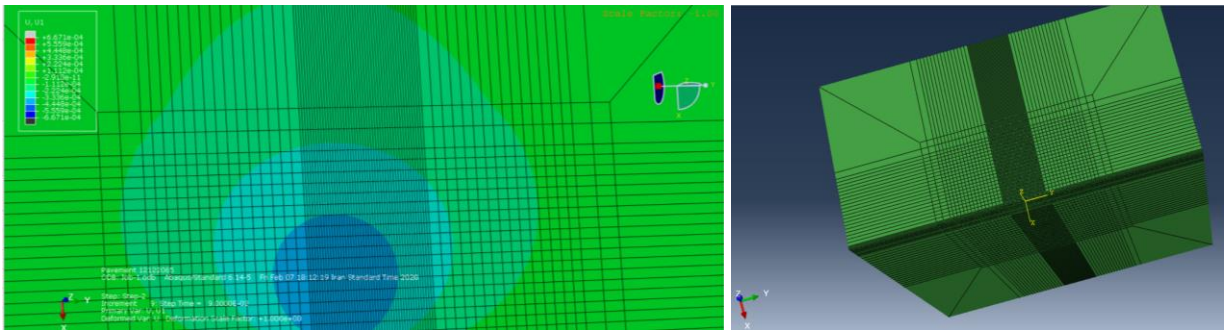

Fig. 3. 3D Abaqus model.

3.1. Verification

ABAQUS carried out the design for all general modeling and not only for the pavement, prior to rely on simulation output needed to verify them compare to real data. In this study, Sebaaly et al field testing results have been used to validate the finite element model [27]. This experiment was performed to investigate the effect of velocity and load magnitude on the tensile strain under the asphalt layer. Then, the strain values were recorded after load passing at 32, 56, and 80 km/h. For this purpose, the sensors were installed under the asphalt layer, and vehicles allowed to pass with three speed. Figure 4 shows the acceptable accuracy between field result and ABAQUS simulations output at three different speeds in the same condition.

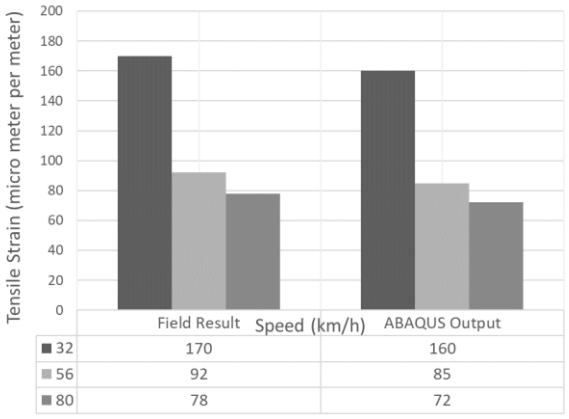

Fig. 4. Comparison of filed result and Abaqus output.

4 .ANN modeling

Computers have revolutionized data processing and turned calculation from traditional to modern operation. Artificial neural networks (ANNs) are a new model of the man central nervous system to simulate the decision process [28,29]. The greater advantage of that is, it's learning to estimate complex and unknown functions problems in a reasonable time [6,28–33]. They act as a black box, model-free, and adaptive tools to learn and recognize a significant patterns in data for prediction and optimization [34]. Hence, after the network has learned the relationship between inputs and outputs, it can calculate solutions and outputs which is close to the desired output [35,36].

The ANNs consist of three layers: an input layer for entering the data into the network, a layer with hidden neurons for predicting relevance between input and output data, and, finally, an output layer that calculates the output values [37,38]. The number of the input layer neurons corresponds to the number of learning variables. The neurons present in the successive layers are combined into paths for sending data within the network. Fig. 5 shows the procedure of an artificial neural network used in this study.

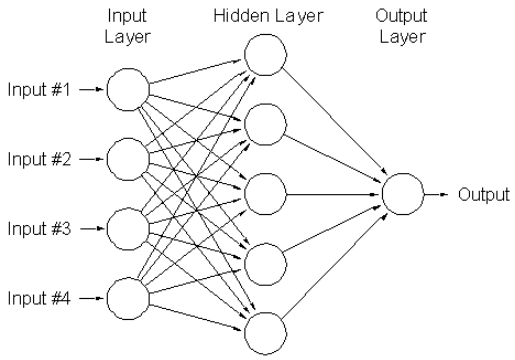

Fig. 5. Artificial neural network procedure.

The main relations of artificial neural networks by McCulloch and Pitts expressed in the following [35].

$$u = \sum_{i=1}^{n} x_i \times w_i - \theta \tag{9}$$

$$y = g(u) \tag{10}$$

Where x_i is the inputs, w_i is the synaptic weights of ith input (ith weight), θ is the Activation threshold or bias, u is the Activation potential (if this value is positive, i.e. if $u \geq \theta$, then the neuron produces an excitatory potential; otherwise, it will be inhibitory), g is the transfer function and y is the output signal.

The transfer function of an Artificial Neural Network describes the main computation performed by a biological neuron and selects from linear, binary step, piecewise linear, sigmoid, Gaussian, and hyperbolic tangent functions [39].

Among all ANN types, backpropagation is a common algorithm for the fitting of weights connection. In this algorithm, the error computed at any step can be sent from the output layer back to the hidden layer and next to the input layer [39–42]. In Backpropagation, there are five types of learning rules: error-correction learning, Boltzmann learning, Hebb learning, competing learning, and perceptron learning [39]. The mean square error function is the usual operation function in the backpropagation network showed in Equation (11).

$$MSE = \frac{1}{mN}\sum_{k=1}^{N}\sum_{j=1}^{m}\left(y_j^k - t_j^k\right)^2 \quad (11)$$

Where m is the output number, and N is the number of training data.

4.1. ANN training

In this survey, between all ANN architectures, the backpropagation algorithm with the non-linear formula for problems selected. As a mentioned, it's one of the most common network not only in transport and pavement modeling; but also predicting different data with disparate architecture and training procedure [39,43–45].

As mentioned, 760 different models resulted from using the ABAQUS simulation has been done to cover all of the possible issues in the EALF. The procedure of EALF calculation depends on various parameters, among them pavement structure number (SN), speed, tire pressure, contact area, axle type, axle length, and final serviceability selected as input layer parameters and EALF as an output of the network. Thus, the input and output arrangement are respectively 7 and 1.

After choosing the properties of the hidden layers, the created transfer function must be defined in every layer. The selected network is consist of sigmoid tangent and simple linear respectively in the hidden and outer layers and could be used a non-linear regression as an appropriate function approximation.

Besides that, there isn't an obvious rule to define the number of hidden layers and their neurons and must be specified due to the minimum acceptable errors in the training and test process. Therefore, the procedure to select an appropriate geometry for the data under consideration has been used for ranging from three layers network to choosing the optimum number of hidden layer neurons. Table 3, with figures 6 and 7, show the regression and error values acquired for three layers networks with different neurons. All ANN modeling was calculated using the MATLAB software.

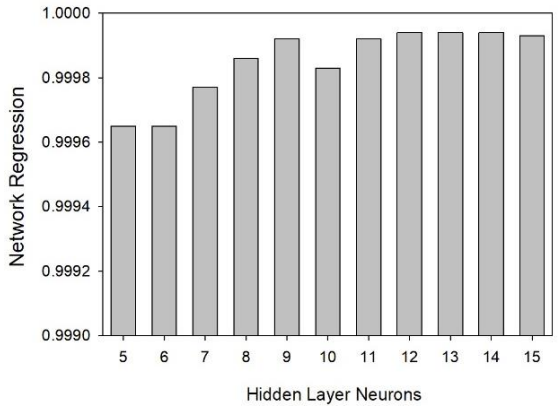

Fig. 6. Finding optimized network based on network regression.

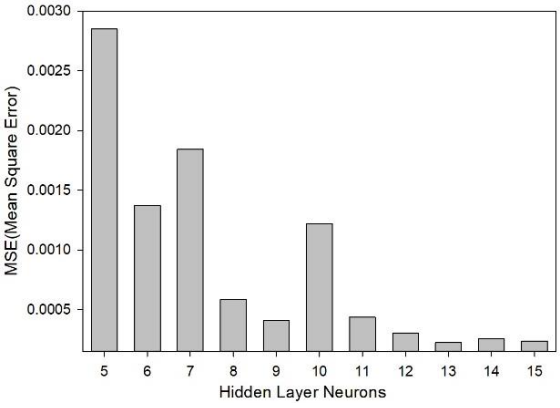

Fig. 7. Finding optimized network based on Mean Square Error.

Table 3. Find optimized network process with neurons changes.

Neurons of hidden layer	Regression				MSE (Mean Square Error)	Epochs
	Training	Validation	Test	All		
5	0.99972	0.99938	0.99972	0.99965	0.00285	757
6	0.99972	0.9997	0.99942	0.99965	0.00137	1000
7	0.99976	0.9996	0.99964	0.99977	0.00184	97
8	0.99986	0.99988	0.99988	0.99986	0.00059	178
9	0.99993	0.99991	0.99991	0.99992	0.00041	98
10	0.99983	0.9997	0.99984	0.99983	0.00122	118
11	0.99994	0.9999	0.9999	0.99992	0.00044	271
12	0.99994	0.99993	0.99992	0.99994	0.00031	264
13	0.99998	0.99986	0.99988	0.99994	0.00022	125
14	0.99994	0.99994	0.99992	0.99994	0.00026	133
15	0.99993	0.99994	0.99993	0.99993	0.00023	233

4.2. Results

An optimum network included low neurons and MSE and high regression in the modeling process [46,47]. Hence, according to the results presented in Table 2 and Figures 6 and 7, the optimum network architecture is 7-13-1. It contains three layers, 7 nodes in the entry layer, an intermediate layer with 13 nodes, and finally, 1 node in the output layer.

In figures 8 and 9, the network regression and the square error values obtained via the training step have been presented. The amount of 0.99998 as the training process regression value confirmed that simulation have a acceptable accuracy with the simulations values. Figure 10 compares the EALF predicted by the Ann network with the results from ABAQUS simulations which shows the high precision of the estimated results.

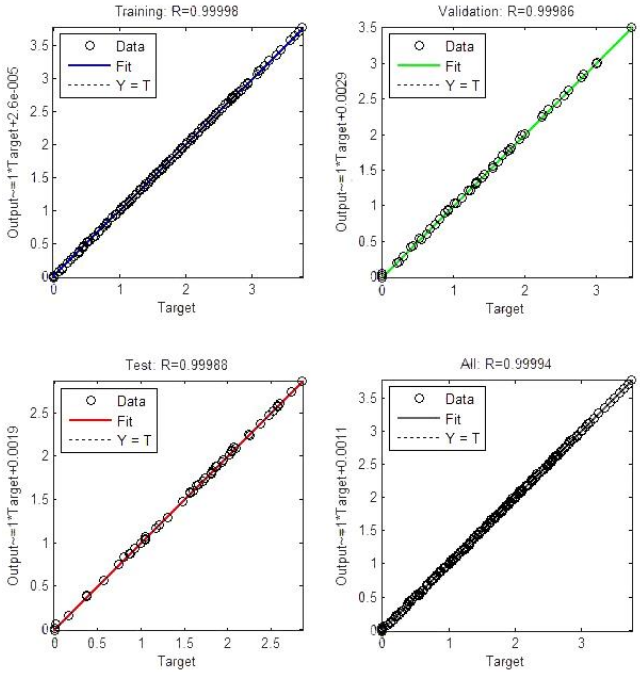

Fig. 8. Selected network regressions in training process.

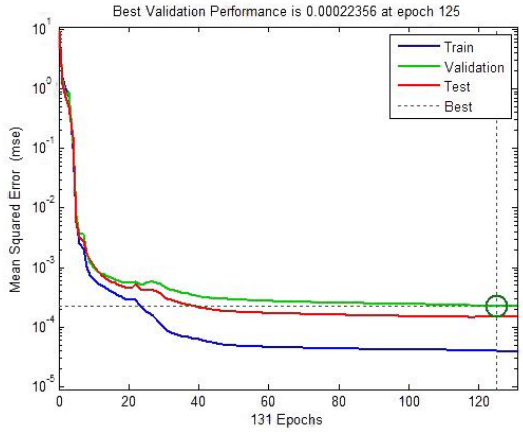

Fig. 9. Selected network Mse in training process.

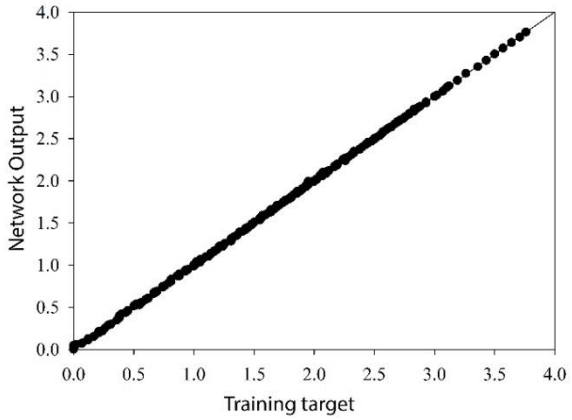

Fig. 10. Quality of the developed Ann.

5 .Conclusions

One of the most important data for pavement design procedure is traffic data, which transformed from traffic spectrum to standard axle and is achieved by Equivalent Axle Load Factor (EALF). Generally, this factor only impressed by the axle type and limited to experimented axles. The effect of the axles like as wheel type (single or dual wheel) and pavement properties was not considered. In this paper, a study conducted based on ANN to define a developed model for EALF calculation. The great advantage of artificial neural networks is high accuracy in solving the planned samples, and elimination of the complex inputs and the capability of model multiple sections in the time unit. The "760 ABAQUS" simulation outputs used for learning data. Pavement structure number (SN), speed, contact area, tire pressure, axle type, axle length, and final serviceability selected for the input layer and EALF based on fatigue criteria choose for the output layer. Finally, a backpropagation network with 7-13-1 architecture and 0.99998 regression is selected as an optimum network.

References

[1] Zaghloul S, White TD. Guidelines for Permitting Overloads; Part 1: Effect of Overloaded Vehicles on the Indiana Highway Network. West Lafayette, IN: 1994.

[2] Chatti K, Lee D, Kim T. Truck Damage Factors Using Dissipated Energy versus Peak Strains. 6th Int. Symp. Heavy Veh. Weight. Dlmensiolns, Saskatoon: 2000, p. 175–83.

[3] Abdel-Motaleb ME. Impact of high-pressure truck tires on pavement design in Egypt. Emirates J Eng Res 2007;12:65–73.

[4] Judycki J. Determination of Equivalent Axle Load Factors on the Basis of Fatigue Criteria for Flexible and Semi-Rigid Pavements. Road Mater Pavement Des 2010;11:187–202.

[5] Chaudry R, Memon AB. Effects of Variation in Truck Factor on Pavement Performance in Pakistan 2013;32:19–30.

[6] Amorim SIR, Pais JC, Vale AC, Minhoto MJC. A model for equivalent axle load factors. Int J Pavement Eng 2014;16:881–93.

[7] Rys D, Judycki J, Jaskula P. Determination of Vehicles Load Equivalency Factors for Polish Catalogue of Typical Flexible and Semi-rigid Pavement Structures. Transp Res Procedia 2016;14:2382–91.

[8] Zhang H, Gong M, Yu T. Modification and application of axle load conversion formula to determine traffic volume in pavement design. Int J Pavement Res Technol 2018;11:582–93.

[9] Singh AK, Sahoo JP. Analysis and design of two layered flexible pavement systems: A new mechanistic approach. Comput Geotech 2020;117:103238.

[10] Deng Y, Luo X, Zhang Y, Lytton RL. Evaluation of flexible pavement deterioration conditions using deflection profiles under moving loads. Transp Geotech 2021;26:100434.

[11] Rezazadeh Eidgahee D, Rafiean AH, Haddad A. A Novel Formulation for the Compressive Strength of IBP-Based Geopolymer Stabilized Clayey Soils Using ANN and GMDH-NN Approaches. Iran J Sci Technol Trans Civ Eng 2020;44:219–29.

[12] Rezazadeh Eidgahee D, Fasihi F, Naderpour H. Optimized Artificial Neural Network for Analyzing Soil-Waste Rubber Shred Mixtures. Sharif J Civ Eng 2015;31.2:105–11.

[13] Rezazadeh Eidgahee D, Haddad A, Naderpour H. Evaluation of shear strength parameters of granulated waste rubber using artificial neural networks and group method of data handling. Sci Iran 2019;26:3233–44.

[14] Naderpour H, Rafiean AH, Fakharian P. Compressive strength prediction of environmentally friendly concrete using artificial neural networks. J Build Eng 2018;16.

[15] Azunna SU, Nwafor EO, Ojobo SO. Stabilization of Ikpayongu laterite using Cement, RHA and Carbide Waste Mixture for Road Subbase and Base Material. Comput Eng Phys Model 2020;3:77–96.

[16] Al-Qadi IL, Wang H, Tutumluer E. Dynamic Analysis of Thin Asphalt Pavements by Using Cross-Anisotropic Stress-Dependent Properties for Granular Layer. Transp Res Rec J Transp Res Board 2010;2154:156–63.

[17] Chen Y. Viscoelastic modeling of flexible pavement. Akron, 2009.

[18] Alkaissi ZA. Effect of high temperature and traffic loading on rutting performance of flexible pavement. J King Saud Univ - Eng Sci 2020;32:1–4.

[19] Zaghloul SM, White T. Use of a three-dimensional, dynamic finite element program for analysis of flexible pavement. Transp Res Rec 1993.

[20] Zarei B, Shafabakhsh GA. Dynamic Analysis of Composite Pavement using Finite Element Method and Prediction of Fatigue Life 2018;04:33–7.

[21] Huang YH. Pavement Analysis and Design. Second Edi. Pearson Education; 2004.

[22] Kim M. Three-Dimensional Finite Element Analysis Of Flexible Pavements Considering Nonlinear Pavement Foundation Behavior. University of Illinois, 2007.

[23] Cebon D. Handbook of vehicle-road interaction. 1999.

[24] Boulos Filho P, Raymundo H, Machado ST, Leite ARCAP, Sacomano JB. CONFIGURATIONS OF TIRE PRESSURE ON THE PAVEMENT FOR COMMERCIAL VEHICLES: CALCULATION OF THE 'N' NUMBER AND THE CONSEQUENCES ON PAVEMENT PERFORMANCE. Indep J Manag Prod 2016;7:584–605.

[25] Filho PB, Raymundo H, Machado ST, Leite ARCAP, Sacomano JB. Configurations of tire pressure on the pavement for commercial vehicles: calculation of the n number and the consequences on pavement performance. Indep J Manag Prod 2016;7:584–605.

[26] Uddin W, Garza S. 3D-FE Modeling and Simulation of Airfield Pavements Subjected to FWD Impact Load Pulse and Wheel Loads. Airf. Pavements, Reston, VA: American Society of Civil Engineers; 2004, p. 304–15.

[27] Sebaaly P, Tabatabaee N, Kulakowski B, Scullion T. Instrumentation for Flexible Pavements-Field Performance of Selected Sensors Volume I : Final Report. vol. I.

1992.

[28] Solatifar N, Lavasani SM. Development of An Artificial Neural Network Model for Asphalt Pavement Deterioration Using LTPP Data. J Rehabil Civ Eng 2020;8:121–32.

[29] Abbaszadeh MA, Sharbatdar M. Modeling of Confined Circular Concrete Columns Wrapped by Fiber Reinforced Polymer Using Artificial Neural Network. J Soft Comput Civ Eng 2020;4:61–78.

[30] LeCun Y, Bengio Y, Hinton G. Deep learning. Nature 2015;521:436–44.

[31] Moradi E, Naderpour H, Kheyroddin A. An artificial neural network model for estimating the shear contribution of RC beams strengthened by externally bonded FRP. J Rehabil Civ Eng 2018;6:88–103.

[32] Darvishan E. The Punching Shear Capacity Estimation of FRP-Strengthened RC Slabs Using Artificial Neural Network and Group Method of Data Handling. J Rehabil Civ Eng 2021;9:102–13.

[33] Naderpour H, Nagai K, Fakharian P, Haji M. Innovative models for prediction of compressive strength of FRP-confined circular reinforced concrete columns using soft computing methods. Compos Struct 2019;215:69–84.

[34] Adeli H. Neural Networks in Civil Engineering: 1989-2000. Comput Civ Infrastruct Eng 2001;16:126–42.

[35] da Silva IN, Hernane Spatti D, Andrade Flauzino R, Liboni LHB, dos Reis Alves SF. Artificial Neural Network Architectures and Training Processes. Artif. Neural Networks, Cham: Springer International Publishing; 2017, p. 21–8.

[36] Abdulla NA. Using the artificial neural network to predict the axial strength and strain of concrete-filled plastic tube. J Soft Comput Civ Eng 2020;4:63–86.

[37] Gajewski J, Sadowski T. Sensitivity analysis of crack propagation in pavement bituminous layered structures using a hybrid system integrating Artificial Neural Networks and Finite Element Method. Comput Mater Sci 2014;82:114–7.

[38] Ghasemi M, Roshani GH, Roshani A. Detecting Human Behavioral Pattern in Rock, Paper, Scissors Game Using Artificial Intelligence. Comput Eng Phys Model 2020;3:25–35.

[39] Profillidis VA, Botzoris GN. Modeling of Transport Demand. Elsevier; 2018.

[40] Naderpour H, Rezazadeh Eidgahee D, Fakharian P, Rafiean AH, Kalantari SM. A new proposed approach for moment capacity estimation of ferrocement members using Group Method of Data Handling. Eng Sci Technol an Int J 2020;23:382–91.

[41] Kanchidurai S, Krishnan PA, Baskar K. Compressive Strength Estimation of Mesh Embedded Masonry Prism Using Empirical and Neural Network Models. J Soft Comput Civ Eng 2020;4:24–35.

[42] Priyadarshee A, Chandra S, Gupta D, Kumar V. Neural Models for Unconfined Compressive Strength of Kaolin Clay Mixed with Pond Ash, Rice Husk Ash and Cement. J Soft Comput Civ Eng 2020;4:85–102.

[43] Hagan MT, Demuth HB, Beale MH, De Jess O. Neural network design. 2nd ed. USA: Martin Hagan; 2014.

[44] Jahangir H, Rezazadeh Eidgahee D. A new and robust hybrid artificial bee colony algorithm – ANN model for FRP-concrete bond strength evaluation. Compos Struct 2021;257:113160.

[45] Kalman Sipos T, Parsa P. Empirical Formulation of Ferrocement Members Moment Capacity Using Artificial Neural Networks. J Soft Comput Civ Eng 2020;4:111–26.

[46] Angus JE. Criteria for choosing the best neural network. Sandiego: 1991.

[47] Papadimitropoulos VC, Tsikas PK, Chassiakos AP. Modeling the Influence of Environmental Factors on Concrete Evaporation Rate. J Soft Comput Civ Eng 2020;4:79–97.